Konya Mühendislik Bilimleri Dergisi., c. 13, s. 4, 1175-1192, 2025
Konya Journal of Engineering Sciences v. 13, n. 4, 1175-1192, 2025
ISSN: 2667-8055 (Electronic)
DOI: 10.36306/konjes.1729516

HYDROTHERMALLY SYNTHESIZED Fe_3O_4 MAGNETIC NANOPARTICLES AS EFFICIENT CATALYST FOR REUSABLE HYDROGEN GENERATION VIA $NaBH_4$ METHANOLYSIS

[1] **Ayhan Abdullah CEYHAN**, [2,*] **Houssem LAKHALI**, [3] **Ömer ŞAHİN**

[1, 2] *Konya Technical University, Engineering and Natural Sciences Faculty, Chemical Engineering Department, Konya, TÜRKİYE*
[3] *Istanbul Technical University, Chemical Metallurgical Engineering Faculty, Chemical Engineering Department, Istanbul, TÜRKİYE*
[1] aaceyhan@ktun.edu.tr, [2] lakhalihoussem91@gmail.com , [3] omersahin@itu.edu.tr

Highlights

- Fe_3O_4 NPs were synthesized as a catalyst to investigate hydrogen generation.
- Hydrogen generation was evaluated via $NaBH_4$ methanolysis under varying conditions.
- At 30 °C, a HGR of 2721.9 $mlg_{cat}^{-1}min^{-1}$ was achieved, with an E_a of 27.18 $kJmol^{-1}$.
- Catalyst retained 99% efficiency after six reuse cycles.

Graphical Abstract

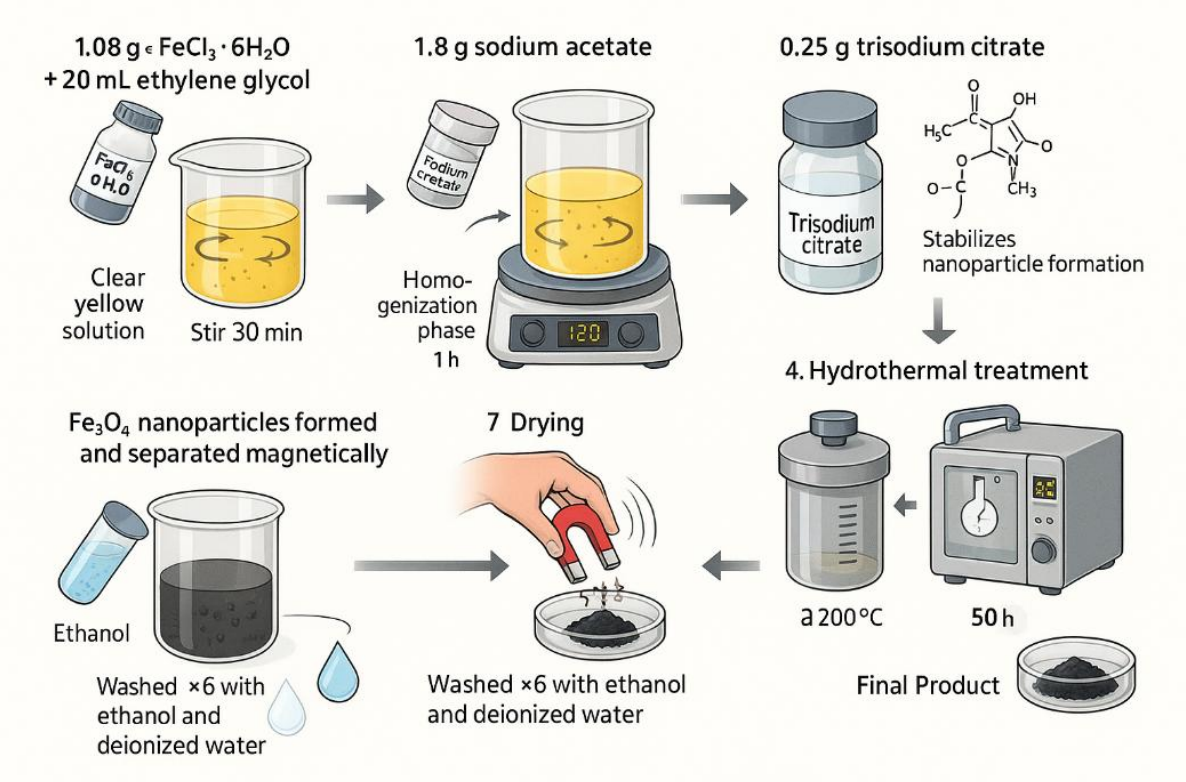

***Corresponding Author:** Houssem LAKHALI, lakhalihoussem91@gmail.com

Konya Mühendislik Bilimleri Dergisi., c. 13, s. 4, 1175-1192, 2025
Konya Journal of Engineering Sciences v. 13, n. 4, 1175-1192, 2025
ISSN: 2667-8055 (Electronic)
DOI: 10.36306/konjes.1729516

HYDROTHERMALLY SYNTHESIZED Fe_3O_4 MAGNETIC NANOPARTICLES AS EFFICIENT CATALYST FOR REUSABLE HYDROGEN GENERATION VIA $NaBH_4$ METHANOLYSIS

[1] Ayhan Abdullah CEYHAN, [2,] * Houssem LAKHALI, [3] Ömer ŞAHİN

[1, 2] Konya Technical University, Engineering and Natural Sciences Faculty, Chemical Engineering Department, Konya, TÜRKİYE
[3] Istanbul Technical University, Chemical Metallurgical Engineering Faculty, Chemical Engineering Department, Istanbul, TÜRKİYE
[1] aaceyhan@ktun.edu.tr, [2] lakhalihoussem91@gmail.com , [3] omersahin@itu.edu.tr

(Received: 30.06.2025; Accepted in Revised Form: 05.08.2025)

ABSTRACT: Herein, we synthesized hydrothermally Fe_3O_4 nanoparticles (NPs) and investigated their catalytic performance in $NaBH_4$ methanolysis for hydrogen generation. Key parameters, including the $NaBH_4$ concentration, catalyst loading, and temperature, were optimized. Comprehensive characterization via XRD,SEM, EDX, FTIR, and BET revealed the surface properties of the catalyst. The optimized catalyst exhibited an outstanding HGR of 2721.9 ml g_{cat}^{-1} min^{-1} at 30°C with an E_a of 27.18 kJ mol^{-1}. FE-SEM analysis indicated particle agglomeration with a size distribution of 200 nm, whereas the BET data demonstrated a moderate surface area of 37.17 m^2 g^{-1} and pore diameter of 13.24 nm. Remarkably, the catalyst maintained 99% efficiency after six reuse cycles, emphasizing its industrial viability and long-term stability.

Keywords: *Magnetic Catalyst, $NaBH_4$, Hydrothermal Method, Hydrogen, Methanolysis*

1. INTRODUCTION

Energy systems, power businesses, transportation, and homes worldwide have traditionally relied on fossil fuels, such as coal, natural gas, and petroleum. However, resource depletion and environmental repercussions are two major problems caused by their overuse. Notably, the burning of fossil fuels is one of the main causes of greenhouse gas emissions, which have increased global temperatures by approximately 1°C over the past century [1]. Fossil fuel combustion is a major source of environmental degradation owing to the continued emission of pollutants, such as sulfur oxides, nitrogen oxides, and aromatic hydrocarbons, which directly contribute to air pollution [1].

As part of global efforts to combat climate change, countries are striving to achieve the ambitious goal of limiting the global temperature rise to 1.5°C above the pre-industrial levels, with a commitment to not exceed 2°C [2]. Hydrogen is gaining prominence as an alternative source within the framework of the transition to cleaner energy, which is a prerequisite for achieving the goals of limiting the global temperature rise.

Hydrogen offers significant advantages, including zero carbon emissions, non-toxicity, and abundant availability of resources. Furthermore, its combustion generates a substantial amount of heat, ranging from 120 to 142 MJ kg^{-1}, significantly surpassing that of other fuels such as natural gas (~42–55 MJ kg^{-1}), petrol (~44–46 MJ kg^{-1}), and wood (~16 MJ kg^{-1}) [3], [4]. Despite these benefits, hydrogen transportation and storage pose major challenges that limit their widespread adoption.

Hydrogen storage methods are widely characterized as physical storage systems, including high-pressure and cryogenic tanks, and material-based storage systems, such as adsorption on carbon nanotubes or activated carbon, and chemical and metal hydrides [5], [6]. Although physical storage systems offer high storage capacities through hydrogen adsorption via van der Waals forces, they require extremely low temperatures, rendering them costly and less practical [7], [8].

In contrast, chemical hydrides are a compelling alternative for long-term hydrogen storage. Formic acid, hydrazine hydrates, metal boron hydrides, aromatic compounds, and ammonia borane are stable

***Corresponding Author:** Houssem LAKHALI, lakhalihoussem91@gmail.com

under ambient conditions, have high hydrogen storage capacities, and are suitable for industrial applications [7], [9], [10].

Sodium borohydride ($NaBH_4$) has recently gained widespread attention as an effective hydrogen storage chemical owing to its outstanding properties, including high stability under normal conditions, low production cost, ease of storage, non-hazardous characteristics, low reaction initiation temperature, hydrogen output with minimal impurities, and good rate control. It also has a theoretical hydrogen storage capacity of 10.8 wt %, and its reaction products are environmentally friendly. $NaBH_4$ is typically produced using the Brown-Schlesinger and Bayer processes [3], [11], [12].

One of the most notable applications of $NaBH_4$ in fuel cell technology was demonstrated in 2001, when the Millennium Cell Corporation successfully integrated it into Daimler Chrysler's fuel cell concept minivan. This breakthrough showcased $NaBH_4$ as a viable alternative to conventional hydrogen storage methods, addressing the safety and efficiency concerns associated with high-pressure hydrogen storage [13].

Hydrogen is generated from sodium borohydride ($NaBH_4$) via hydrolysis and breakdown in methanol at room temperature. Both reactions can be carried out under mild environmental conditions, as shown in Equations (1) and (2).

$$NaBH_4 + (2+x)\,H_2O \xrightarrow{catalyst} 4H_2 + NaBO_2.xH_2O + heat \quad \Delta H = -217\ kJmol^{-1} \tag{1}$$

$$NaBH_4 + 4\,CH_3OH \xrightarrow{catalyst} 4H_2 + NaB(OCH_3)_4 + heat \tag{2}$$

Notably, the byproducts of these reactions, $NaBO_2$ and $NaB(OCH_3)_4$, can be recycled to synthesize $NaBH_4$, significantly reducing production costs. Methanolysis offers unique advantages, including operation at subzero temperatures (as low as −97.6 °C) and atmospheric pressure. Unlike $NaBO_2$, $NaB(OCH_3)_4$ does not clog the reactors, making methanolysis particularly advantageous. Furthermore, methanolysis provides a moderate gravimetric hydrogen storage capacity of 4.9 wt%[14], [15], [16].

Recent progress in $NaBH_4$ methanolysis has emphasized the design and application of diverse catalytic systems, which can broadly categorized into: (i) transition metal-based catalysts, such as cobalt [17], Ni-based catalysts [18], Cu-based catalysts [19] , etc.), (ii) noble metal-based catalysts, including ruthenium [20], Pt-based catalysts [21], etc.), and (iii) alloy and composite catalysts, such as carbon nanotube-supported metals [22], and hybrid frameworks like ZIF-67@graphene [23], etc.). These catalysts have been extensively investigated to enhance hydrogen generation efficiency by improving their activity, stability, and cost-effectiveness.

Among these, Fe_3O_4-based catalysts are cost-effective, nontoxic, biocompatible, and exhibit high magnetic saturation and superparamagnetic properties. Additionally, Fe_3O_4 nanoparticles can be easily recovered magnetically, thereby enhancing their reusability [24], [25], [26], [27].

For example, the CoNi/Fe_3O_4@GO catalyst was synthesized via an impregnation-reduction approach, achieving an HGR of 8200 ml g_{cat}^{-1} min^{-1} during the reaction. Their thermodynamic and kinetic analyses revealed an activation entropy of -97.75 J K^{-1} and an activation energy of 21.45 kJ mol^{-1}, highlighting the effectiveness of the catalyst in hydrogen production through a Langmuir-Hinshelwood-type mechanism [28]. Similarly, Alshammari et al. developed Fe_3O_4/FeS_2/g-C_3N_4 nanocomposites using a sol-gel method, with the 3.0 wt% Fe_3O_4/FeS_2/g-C_3N_4 nanosheet attaining a remarkable HGR of 8480 ml g_{cat}^{-1} min^{-1} [29].

This study presents a novel approach employing Fe_3O_4-based catalysts for hydrogen production through sodium borohydride methanolysis, offering a cost-effective and affordable substitute for non-transition catalysts. Unlike expensive catalysts such as Pt, Ru, or Pd, Fe_3O_4 is abundant, low-cost, and magnetically recoverable, making it very useful in applied settings. This study systematically investigated key reaction parameters, including catalyst dosage, $NaBH_4$ concentration, reaction temperature, and catalyst reusability, to provide a comprehensive understanding of Fe_3O_4's catalytic performance.

Advanced diagnostic techniques, including field emission scanning electron microscopy (FE-SEM) with energy dispersive X-ray (EDX), FTIR spectroscopy, BET surface area and pore capacity analysis, and X-ray diffraction (XRD), were used to accurately study the structural and functional properties of the catalyst, elucidating how its morphology, composition, and surface area influence catalytic activity.

A key novelty of this study is the exploration of Fe_3O_4's magnetic recoverability, which allows for efficient separation and reuse, thereby enhancing catalyst longevity and sustainability. Furthermore, this study evaluated the stability of Fe_3O_4 over multiple reaction cycles, addressing the challenges related to catalyst durability and performance retention. These findings contribute to the development of scalable and practical hydrogen generation systems, making Fe_3O_4 a viable alternative for clean energy applications such as fuel cells and renewable energy storage.

2. MATERIALS AND METHODS

2.1. Materials

Merck provided iron chloride hexahydrate, sodium borohydride ($NaBH_4$), cobalt(II) chloride hexahydrate, ethanol (≥95%), the sodium salt of acetic acid, ethylene glycol (EG), and trisodium citrate. The University of Selçuk provided the distilled water.

2.2. Fe_3O_4 NPs synthesis

Fe_3O_4 NPs were synthesized using a hydrothermal technique adapted from a previously reported procedure [30]. In a preliminary step, 1.08 g of ferrous chloride hexahydrate was placed in 20 ml of ethylene glycol and dissolved using magnetic stirring. After 30 min, the mixture transitioned to a yellow color. Next, 1.8 g of sodium acetate was added, and the mixture was stirred for an additional hour to achieve a homogeneous solution. To further stabilize the dispersion, the necessary amount of trisodium citrate was added to the mixture. The resulting uniform dispersion was transferred to a hydrothermal reactor and maintained at 200 °C for 10 h. Upon completion, the black magnetic particles were separated in a magnetic field and thoroughly washed with a mixture of ethanol and DI water. Finally, the product was vacuum-dried for 12 h at 50 °C to produce pure Fe_3O_4 nanoparticles.

2.3. Generation of hydrogen from methanolysis process

Hydrogen generation experiments were conducted using a reaction vessel connected to a device for capturing the generated gases. The system included an outlet tube connected to an inverted gas urea tube filled with water to ensure accurate gas volume measurements. Pre-mixed $NaBH_4$ and NaOH solutions were introduced into a flask containing the catalyst to ensure uniform reaction kinetics by avoiding agitation. A hydrogen displacement with water, in which the amount of hydrogen generated was exactly proportional to the volume displaced, was used (Fig. 1).

The initial investigation of $NaBH_4$ methanolysis was carried out using a solution of 1.5% $NaBH_4$, 100 mg of catalyst, and 10 ml of solution, maintained at 30 °C.

2.4. Characterization

Brunauer–Emmett–Teller (BET), Field Emission Scanning Electron Microscopy (FE-SEM), Energy Dispersive X-Ray Spectroscopy (EDX), X-Ray Diffraction (XRD), and Fourier Transform Infrared Spectroscopy (FTIR) were employed to characterize the produced catalyst. To identify the functional groups (4000-400 cm^{-1}), an FTIR spectrometer (Thermo Scientific Nicolet 380) was used. The catalyst's structure was studied using FE-SEM, and elemental analysis was done using EDX (Zeiss Sigma 300) equipment. The synthesized catalysts' crystal structure and phase purity were assessed using XRD diffraction (Bruker D8 Advance). The catalyst's surface area was examined using a BET device (Quantachrome Nova 1200).

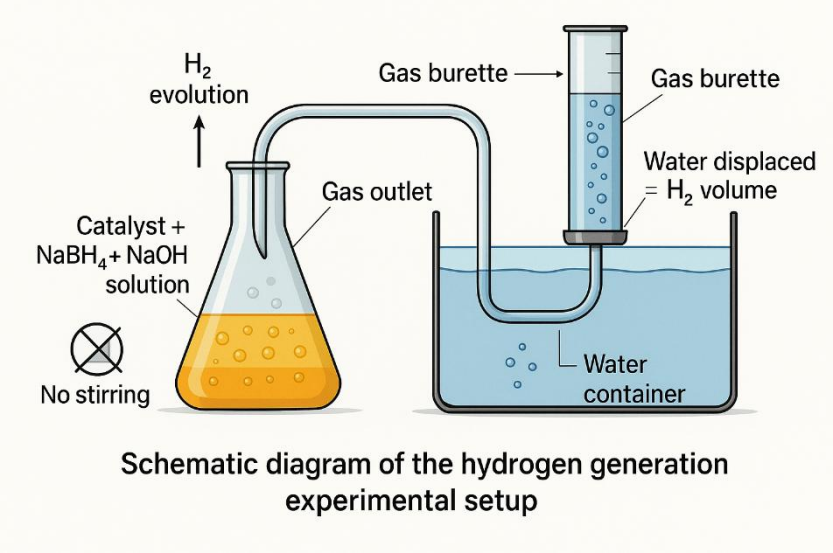

Figure 1. The mechanism of Generation of Hydrogen

3. RESULTS AND DISCUSSION

3.1. X- ray diffraction (XRD) analysis

XRD analysis was used to investigate the structure and phase purity of the Fe_3O_4 NPs. The diffraction patterns (Fig. 2) exhibited prominent peaks at 2θ = 30.21° (220), 35.57° (311), 43.25° (400), 53.71° (422), 57.21° (511), and 62.83° (440). These results confirm the effective synthesis of Fe_3O_4 nanoparticles (NPs), which match the standard pattern of Fe_3O_4 according to JCPDS Card No. 65-3107 and may be indexed to the cubic space group Fd3m[31]. To further investigate the structural properties of the powdered nanoparticles, parameters such as the lattice constant, crystallite size, and full width at half maximum (FWHM) were analyzed using the OriginPro 2025 software (Table 1). The calculated lattice parameters for Fe_3O_4 were consistent across crystallographic planes, with values of a=c, in agreement with previously reported findings [32], [33].

The Debye-Scherrer equation was used to calculate the average crystallite size (Equation 3) [34]:

$$d=\frac{0.9\,\lambda}{\beta\,cos\theta} \quad (3)$$

where λ is the wavelength of the X-ray source (0.1541 nm), β is the FWHM, d is the diameter of particle, k is the shape factor (0.9). The crystallite size of the synthesized sample was determined to be around 10.35 nm. Furthermore, specific calculations of the (311) diffraction plane yielded a crystallite size of 8.91 nm.

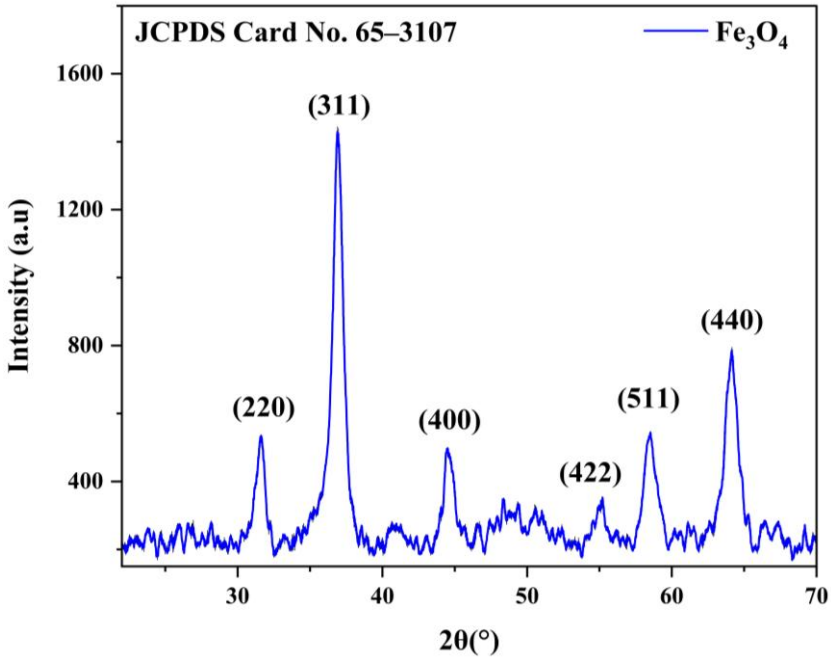

Figure 2. XRD pattern of the synthesized Fe_3O_4 NPs

Table 1. Properties analysis of Fe_3O_4

2θ(°)	(hkl)	Intensity (a	FWHM (°)	d (hkl)	a	c	d(nm)	d moy. (nm)
31.56	(220)	215.01	0.715	0.283	0.57	0.56	11.53	
36.92	**(311)**	**1113.87**	**0.939**	**0.243**	**0.49**	**0.48**	**8.91**	
44.59	(400)	211.72	0.779	0.203	0.41	0.40	11.01	**10.35**
55.06	(422)	72.562	0.701	0.166	0.34	0.33	12.76	
58.50	(511)	304.80	0.979	0.157	0.32	0.31	9.293	
64.11	(440)	590.51	1.089	0.145	0.29	0.29	8.605	

3.2. Field Emission Scanning Electron Microscopy (FE-SEM- EDX) analysis

The morphology of the Fe_3O_4 nanoparticles was assessed using FE-SEM imaging, and the elemental composition was investigated by EDX analysis.

As shown in the FE-SEM image (Fig. 3-a), the prepared catalyst exhibited a spherical shape in terms of morphological structure, with a particle size distribution ranging from 150 to 250 nm [35].

However, significant particle aggregation was also observed. This can be explained by the strong magnetic interactions between individual nanoparticles [36]. The highly aggregated particles further indicate a pore-free crystalline structure, consistent with previous findings [37].

The EDX spectrum (Fig. 3-b) and Table 2 confirm that the nanoparticles were composed of Fe (66.7 wt%) and O (33.3 wt%).

The corresponding EDX mapping (Fig. 3-c) confirms the spatial distribution of Fe and O across the sample, validating the catalyst synthesis. The bright green regions in the EDX map, which are indicative of high Fe concentrations, corroborate the formation of Fe-rich Fe_3O_4 structures. Although the homogeneous distribution of elements indicates a high degree of purity, the localized clustering observed in certain areas suggests nanoparticle aggregation, a phenomenon commonly associated with the high surface energy of nanoscale materials.

Nevertheless, the EDX analysis confirmed the stoichiometric integrity and structural uniformity of the Fe_3O_4 nanoparticles. These results highlight the potential of the synthesized Fe_3O_4 nanoparticles for various applications, including catalysis, hydrogen generation, and magnetic technology.

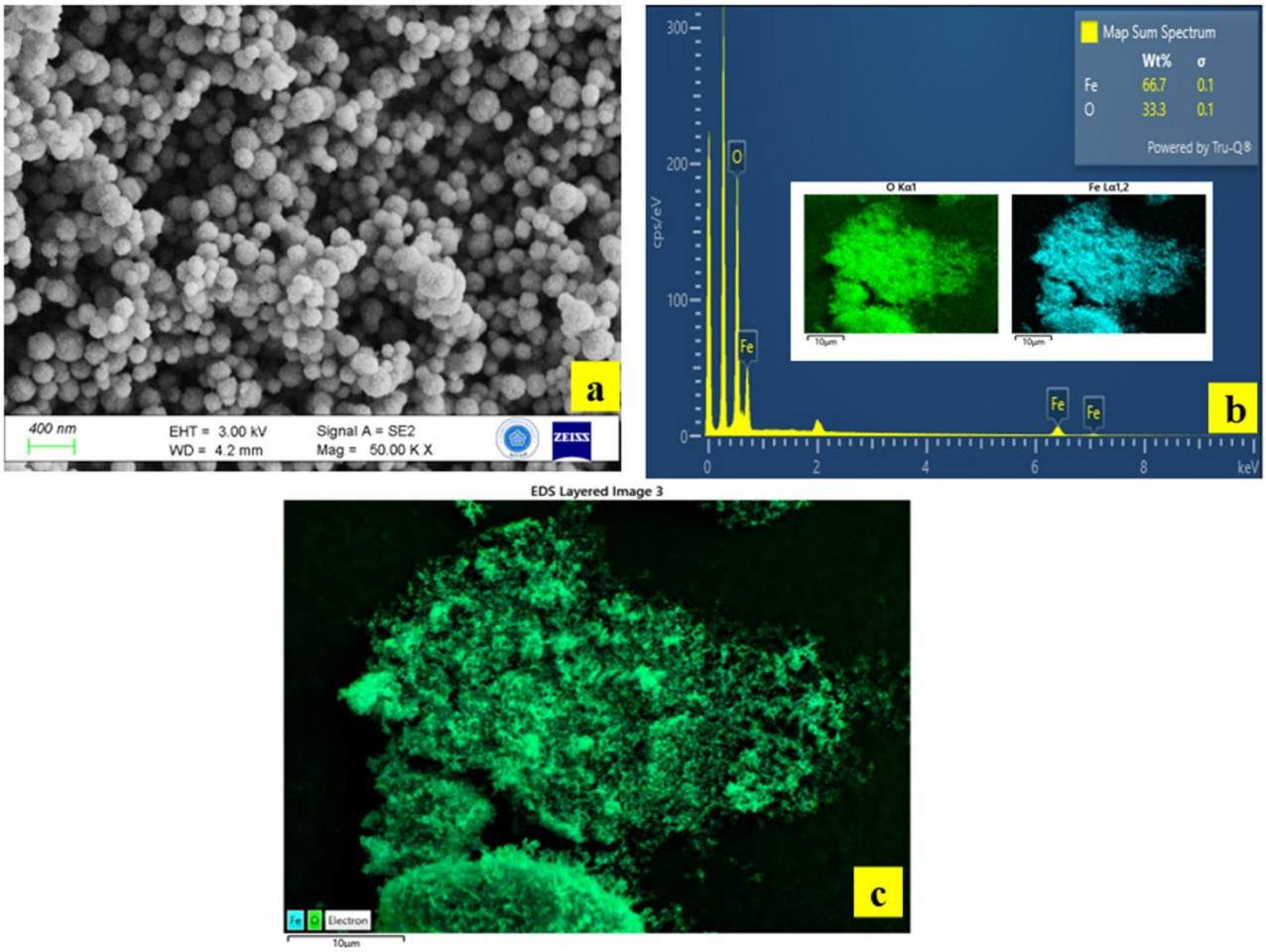

Figure.3. FESEM image (a) -EDX spectrum (b) - EDX map (c) of the synthesized Fe_3O_4 NPs

3.3. Fourier Transform Infrared Spectroscopy (FTIR) analysis

The functional groups in the synthesized catalysts were identified using FTIR spectroscopy. The FTIR spectrum depicted in Fig. 4 reveals several characteristic peaks that provide insights into the chemical structure of the material.

The wide absorption band at approximately 580 cm^{-1} is associated with the stretching vibrations of Fe–O, confirming the presence of Fe_3O_4 nanoparticles [38], [39]. A distinct peak at 1056 cm^{-1} indicates C–O stretching vibrations, whereas those at ~1480 cm^{-1} are attributed to the deformational vibrations of adsorbed water molecules (-OH) [40]. Additionally, the absorptions observed at 1628.4 cm^{-1} and 1389.2 cm^{-1} are assigned to the COO^-–Fe bond. These peaks suggest that the OH- groups on the Fe_3O_4 NPs surface reacted with the carboxylate anion of sodium citrate, successfully grafting sodium citrate onto the Fe_3O_4 nanoparticles [41]. Finally, the peak at 3239 cm^{-1} confirms the presence of O–H stretching vibrations, indicative of hydroxyl groups within the catalyst structure [42], [43]. This comprehensive FTIR analysis validates the functionalization of Fe_3O_4 nanoparticles and provides essential insights into the chemical modifications achieved during the synthesis process.

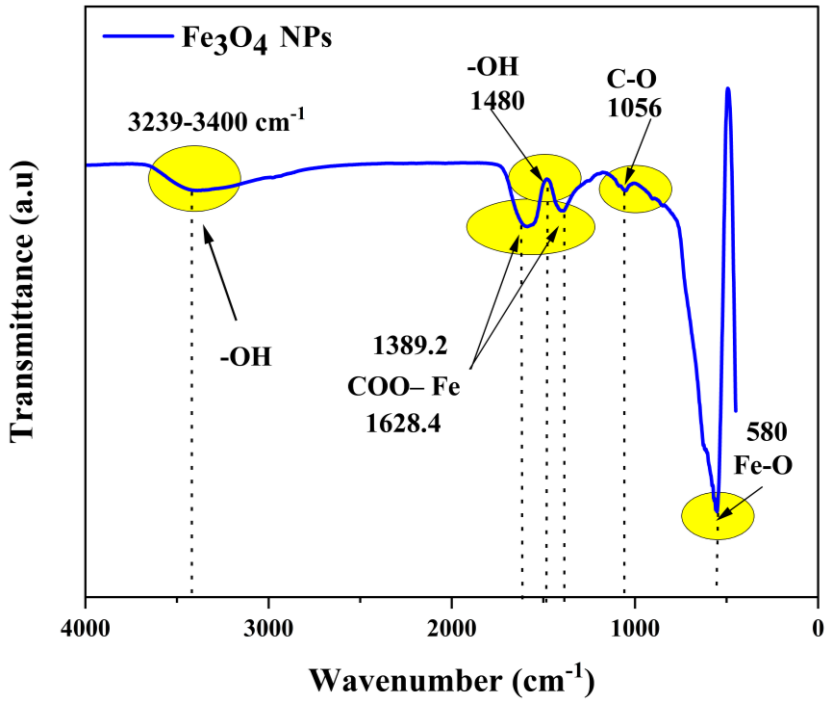

Figure 4. FTIR spectrum of of the synthesized Fe_3O_4 NPs

3.4. Brunauer–Emmett–Teller (BET) analysis

BET analysis was conducted to evaluate the surface area and pore characteristics of the synthesized Fe_3O_4 NPs.

The catalyst had a pore volume of 0.06 $cm^3\ g^{-1}$ and a surface area of 37.17 $m^2\ g^{-1}$, according to the data provided in Table 3.

To investigate the physical properties, N_2 adsorption-desorption isotherms were analyzed at low temperatures (Fig. 5). According to IUPAC, the isotherms showed a type IVa hysteresis loop, which is typical of mesoporous materials. However, the Fe_3O_4 NPs had a pore volume of 0.06 $cm^3\ g^{-1}$ and a pore diameter of 13.24 nm (Table 2).

These findings align with the essential features of mesoporous materials, further validating the suitability of the synthesized Fe_3O_4 nanoparticles for catalysis and other advanced material applications [44].

Table 2. BET results for of the synthesized Fe_3O_4 NPs

Textural properties (DFT)	**Fe_3O_4**
Surface area ($m^2\ g^{-1}$)	37.17
Pore volume ($cm^3\ g^{-1}$)	0.06
Pore diameter (nm)	13.24

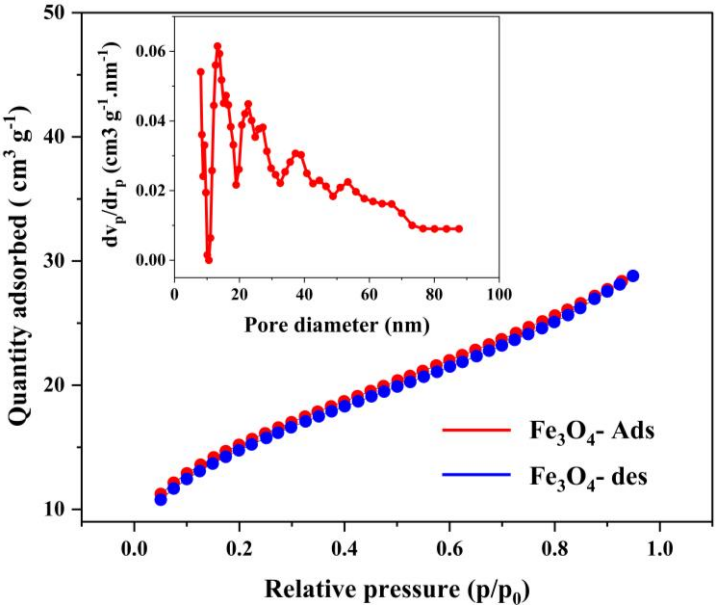

Figure 5. the Fe_3O_4 NPs pore size distribution curves and N_2 adsorption-desorption isotherms.

4. THE PARAMETERS EFFECTS IN $NaBH_4$ METHANOLYSIS REACTION

The Fe_3O_4 NPs were chosen as a suitable catalyst for $NaBH_4$ methanolysis because of their superior hydrogen generation rate (HGR) compared to that of the $Fe_3O_4@SiO_2$ and $Fe_3O_4@SiO_2$/Co-Mo composites. The Fe_3O_4 NPs exhibited the highest HGR of 271.9 ml g_{cat}^{-1} min^{-1}, surpassing $Fe_3O_4@SiO_2$ (2416.86 ml g_{cat}^{-1} min^{-1}) and $Fe_3O_4@SiO_2$/Co-Mo (2120.50 ml g_{cat}^{-1} min^{-1}). As shown in Fig. 6, this indicates that the Fe_3O_4 NPs facilitate more efficient catalytic activity, likely owing to their enhanced surface area, better active site accessibility, and minimal diffusion resistance. Furthermore, their magnetic characteristics facilitate effortless recovery and repurposing, rendering them economical and effective options for producing hydrogen via $NaBH_4$ methanolysis. A detailed explanation of this catalytic effect is provided in the catalytic effect section.

4.1. Media Selection and Its Impact on Hydrogen Generation

In this study, Fe_3O_4 nanoparticles exhibited moderate catalytic activity for the production of hydrogen from $NaBH_4$ in methanol, while showing negligible performance in water (hydrolysis), ethylene glycol, and methanol-ethylene glycol combinations. The pronounced reactivity in methanol can be attributed to its optimal balance of the dielectric constant, proton availability, and low viscosity, which collectively enhance BH_4^- solvolysis via an alcoholysis pathway. Conversely, ethylene glycol (EG), despite being a protic solvent, suffers from high viscosity and reduced proton mobility, which can hinder mass transport and limit the availability of free protons necessary for efficient BH_4^- decomposition [45], [46].

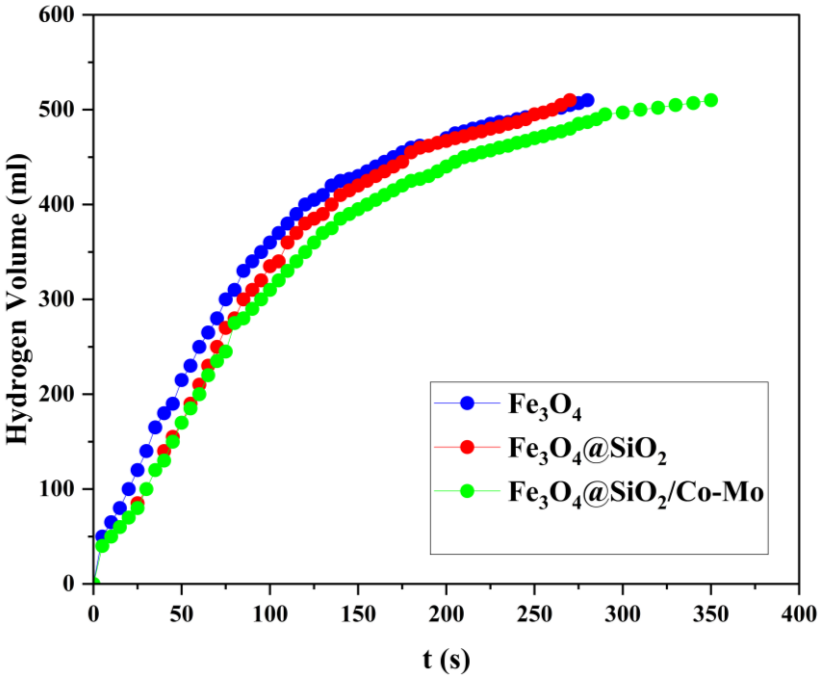

Figure 6. The Hydrogen volume variation with different catalysts

4.2. The NaOH effect on the $NaBH_4$ methanolysis

The influence of NaOH concentration on $NaBH_4$ methanolysis was examined using a loading catalyst of 100 mg, 1.5% $NaBH_4$, and 30 °C. The results indicated that the presence of NaOH adversely affected hydrogen generation, with minimal hydrogen evolution (30–40 ml).

These findings align with those of previous studies, where NaOH significantly reduced the hydrogen generation rate of cobalt-doped catalysts (CEP_{cat}). The observed decrease in hydrogen release is due to competitive adsorption on the catalyst surface. Specifically, OH^- ions are more likely to adsorb onto the surface than BH_4^- ions, thereby inhibiting the interaction of BH_4^- ions with the active centers and consequently lowering the reaction rate [47], [48].

Based on these findings, subsequent experiments were conducted in the absence of NaOH to ensure optimal conditions for hydrogen generation. This adjustment aims to mitigate competitive adsorption effects and enhance the overall catalytic efficiency.

4.3. The $NaBH_4$ effect on the $NaBH_4$ methanolysis

The effect of $NaBH_4$ concentration during methanolysis was tested with a loading catalyst at 30 °C. The $NaBH_4$ concentrations varied between 1.5 and 10%. At 5%, 7%, and 10% $NaBH_4$ concentrations, the theoretical amount of hydrogen gas was not achieved because of by-product precipitation on the surface of the catalyst, which likely inhibited the catalytic activity.

Therefore, 1.5% $NaBH_4$ was selected as the suitable concentration with 100 mg of catalyst for the next step of this study [49], [50], [51].

However, the methanolysis of $NaBH_4$ over the Fe_3O_4 NPs catalyst may proceed through a stepwise mechanism, as shown in Fig. 7 and the following equation.

1) The mechanism starts with the adsorption of BH_4^- ions in methanol onto the catalyst surface of Fe_3O_4 nanoparticles, where electron transfer leads to the production of negatively charged hydrogen hydride (H^-), followed by the formation of an Fe–H bond;

2) Methanol (CH_3OH) then adsorbs onto the iron surface, forming a reactive complex.

3) The hydrogen bound to iron (Fe–H) reacts with the protonated hydrogen (H^+) from the methanol molecule, generating one equivalent of hydrogen gas (H_2), while the methoxide group (CH_3O^-) bonds to the boron atom to form BH_3OCH_3 through the formation of a B–O coordination bond resulting from the donation of an electron pair from the methoxide group to the vacant orbital of the boron atom

4) The reaction continues along a similar pathway until the final compound $NaB(OCH_3)_4$ is formed, accompanied by the production of four molecules of hydrogen gas;

5) Finally, the active sites on the catalyst surface are regenerated after $NaB(OCH_3)_4$ separates from iron [52], [53].

Step	Reactions
1	$NaBH_{4(s)} \rightleftharpoons Na^+_{(aq)} + BH^-_{4(aq)}$
2	$H^+_{(aq)} + BH^-_{4(aq)} \rightleftharpoons BH_{3(s)} + H_{2(g)}$
3	$BH_{3(s)} + 3CH_3OH_{(l)} \rightleftharpoons B(CH_3)_{3(aq)} + 3H_{2(g)}$
4	$B(CH_3)_{3(aq)} + 3CH_3OH_{(l)} \rightleftharpoons B(3CH_3OH)^-_{4(aq)} + H^+_{(aq)}$
5	$4B(CH_3O)^-_{4(aq)} + 2H^+_{(aq)} + 7H_2O_{(l)} \rightleftharpoons B_4O_7^{2-}{}_{(aq)} + 16CH_3OH_{(l)}$

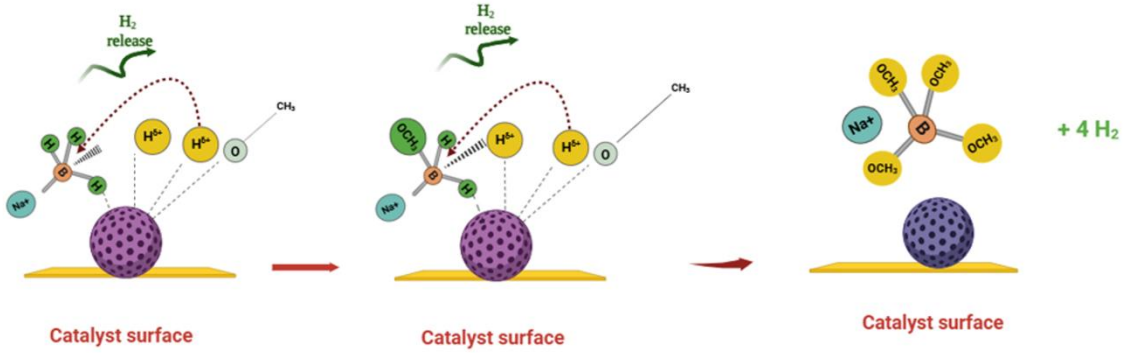

Figure 7. The suggested hydrogen process for the synthesized Fe_3O_4 NPs

4.4.The temperature effect on the $NaBH_4$ methanolysis

The influence of temperature on $NaBH_4$ methanolysis was investigated at 20–50°C using 1.5% $NaBH_4$ and 100 mg of catalyst. The HGR increased from 1865.4 ml g_{cat}^{-1} min^{-1} (20°C) to 5694 ml g_{cat}^{-1} min^{-1} (50°C) (Figure 8). This trend is consistent with the expected behavior of thermally driven chemical reactions. The increase in HGR with temperature is due to the fact that at elevated temperatures, the molecular velocity is enhanced, leading to an increased frequency of collisions between the reactant molecules. Second, elevated temperatures provide the energy necessary to overcome the kinetic stability of intermediates, facilitating internal solvent percolation and accelerating the reaction [54], [55], [56], [57].

4.5. Kinetic analysis

- **n^{th} order model**

Kinetic analyses were performed based on the results of experiments carried out at different temperatures to evaluate the behavior of the Fe_3O_4 catalyst. Thus, the kinetic parameters were found using the nth-order model (Equation 4-6).

$$-r_A = -\frac{AdC_A}{dt} = KnC_A^n \quad (4)$$

where:

r is the hydrogen generation rate (mmol min^{-1}),

C is the concentration of sodium borohydride (mol L^{-1}),
k is the rate constant (dependent on temperature),
n is the reaction order with respect to the $NaBH_4$ concentration.

The reaction order (n) was determined by plotting ln r versus ln C, with the slope corresponding to n. This approach provides insights into the mechanistic aspects of the catalytic hydrolysis/methanolysis reaction pathway.

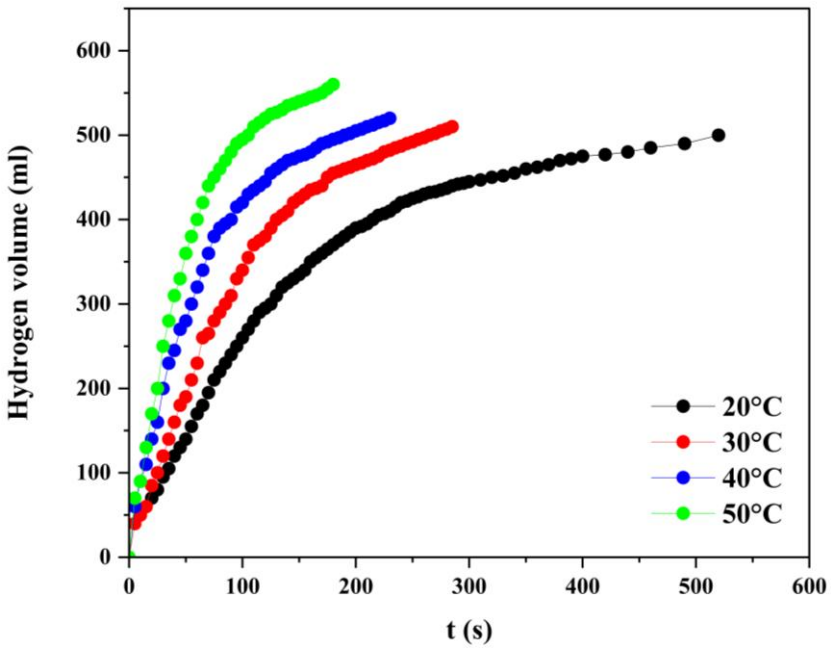

Figure 8. The hydrogen volume evolution with the temperature (1.5% $NaBH_4$, 100 mg catalyst)

By integrating.

$$-\int_{C_{NaBH_4\,0}}^{C_{NaBH_4}} \frac{dC_A}{C_n^A} = \int_0^t dt \quad (5)$$

Finally, we get:

$$\frac{1}{C_{NaBH_4}^{n-1}} = (n-1).k.t + \frac{1}{C_{NaBH_4\,0}^{n-1}} \quad (n\neq1) \quad (6)$$

The E_a of the $NaBH_4$ methanolysis processes can be found by applying the Arrhenius equation (7).

$$\ln k = \ln A - \frac{E_a}{RT} \quad (7)$$

The variation of 1/T with ln k graphic slope in Fig.9-a was used to assess E_a. In this instance, the activation energy of the $NaBH_4$ methanolysis reaction was 27.54 kJ mol^{-1}.

- **Langmuir–Hinshelwood kinetic model**

The activation energy is commonly calculated using the Langmuir–Hinshelwood model (Equation 8).

$$\frac{dC_{NaBH_4}}{dt} = -r.NaBH_4 = -k\,\frac{K_{ads}C_{NaBH_4}}{1+k_{ads}C_{NaBH_4}} \quad (8)$$

The activation energy was calculated using Equation (9), which was obtained by integration.

$$\frac{1}{K_{ads}}.ln\,\frac{NaBH_{4_0}}{NaBH_4} + NaBH_{4_0} - NaBH_4 = -k\,t \quad (9)$$

According to the (1/T) fluctuation with ln(k) graphics in Figure 9-b, 31.70 kJ mol^{-1} was found to be the activation energy.

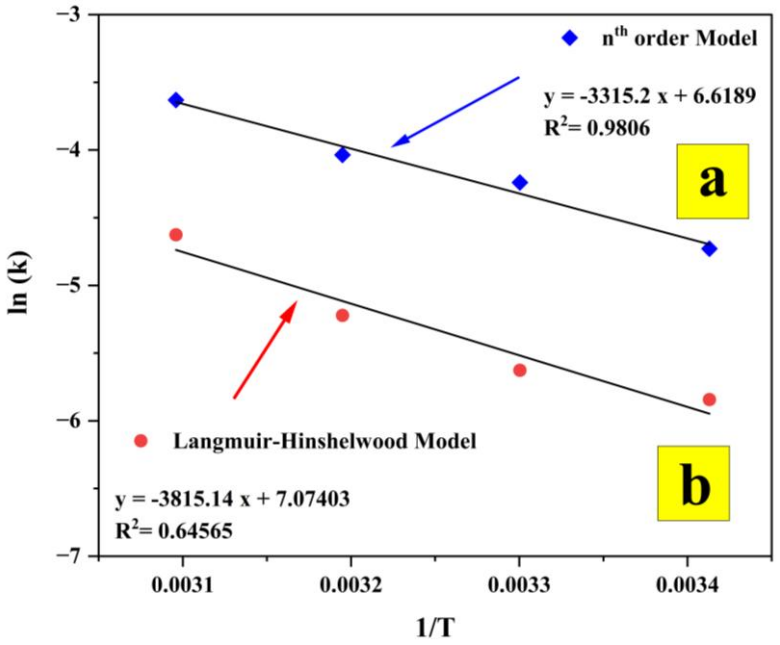

Figure 9. the relationship between (1/T) and ln(k) for the $NaBH_4$ methanolysis for the n^{th} order and Langmuir–Hinshelwood kinetic model

However, the relationship between the (ΔS°) and (ΔH_{ads}) according to the obtained Kads data can be computed using Equation 10, which can be used to calculate ΔG°.

$$\ln K_{ads} = \frac{\Delta S^\circ}{R} - \frac{\Delta H_{ads}}{R}\frac{1}{T} \quad (10)$$

Here, the inverse of the temperature (1/T) illustrates the variation in the adsorption equilibrium with temperature.

According to this method, the slope represents − ΔH_{ads}/R, whereas the intercept corresponds to ΔS°/R.

As shown in Figure 10, the standard entropy change (ΔS°) was determined to be 38.90 ± 0.01 kJ $mol^{-1}K^{-1}$, and the adsorption enthalpy change (ΔH_{ads}) was found to be 45.13 ± 0.01 kJ mol^{-1}.

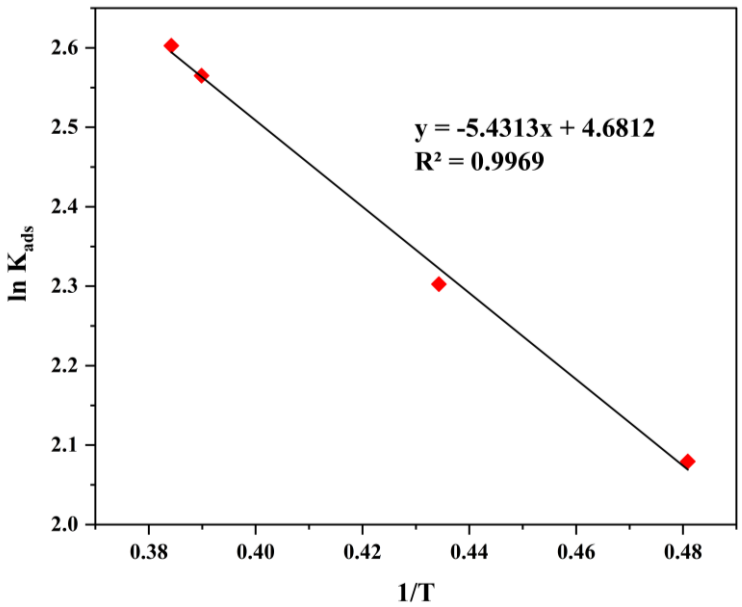

Figure 10. (1/T) variation with ln(K_{ads}) for the $NaBH_4$ methanolysis

However, the ΔG° was calculated via Equation 11 (Table 3).

$$\Delta G^\circ = \Delta H_{ads} - T \cdot \Delta S^\circ \quad (11)$$

Table 3. Overview of the ΔG°, ΔS°, and ΔH_{ads}, values derived from K_{ads} calculations

T	K_{ads}	ΔG° (J·mol^{-1})	ΔS° (kJ·mol^{-1}·K^{-1})	ΔH_{ads} (kJ·mol^{-1})
20°C	13.5	-11352.57		
30°C	13	-11741.57		
40°C	10	-12130.57	38.90± 0.01	45.13 ± 0.01
50°C	8	-12519.57		

- **Turnover Frequency Number (TOF)**

The number of reactant molecules transformed per active site in a specific amount of time is indicated by the TOF.

As shown in Equation 12, it is generally expressed as mol_{H2} mol_{cat}^{-1} h^{-1}.The number of active sites in the response is the main focus of the TOF [58], [59], [60].

$$\text{Turnover Frequency } (mol_{H2}\ mol_{cat}^{-1}\ h^{-1}) = \frac{n_{mol\ H_2}}{catalyst_{\ mol}\ time_{\ h}} \quad (12)$$

A moderate TOF of 604.84 mol_{H2}·mol_{cat}^{-1} h^{-1} was demonstrated by the fabricated sample during $NaBH_4$ methanolysis at 30°C. This corresponded to a HGR of 2721.9 ml g_{cat}^{-1} min^{-1}.

Table 4 compares the catalytic performance of the Fe_3O_4 NPs with that of other catalysts reported in the literature. Our results showed a notable Ea and a remarkably high HGR.

Table 4. Catalytic performance comparison between Fe_3O_4 NPs and in the literature.

Catalyst	Experiments conditions	HGR (ml $g^{-1}min^{-1}$)	Ea (kJ mol^{-1})	Ref
CoNi/Fe_3O_4@GO	15 mg, 3.5% $NaBH_4$	8200	21.45	[61]
Co–Cu–B	15% NaOH, 2.5% $NaBH_4$	270	40.53	[62]
Fe–Ni/MMT	10 ml, 100 mg $NaBH_4$	2480	17.22	[63]
Ru-Fe/GO	1% NaOH, 10% $NaBH_4$	473	59.33	[64]
Fe-B NPs	1% NaOH, 15% $NaBH_4$	5487	7.02	[65]
Fe_3O_4 NPs	100 mg, 10% $NaBH_4$	2721.9	27.18	**This study**

4.6.The reusability of Fe_3O_4 in $NaBH_4$ methanolysis

Experiments were conducted using a loading catalyst of 100 mg, 1.5% $NaBH_4$, and 30 °C to examine the reusability of the Fe_3O_4 NPs while maintaining reliable and consistent conditions.

To remove any remaining byproducts, the catalyst was carefully cleaned with ethanol and deionized water after each test. To prepare it for further cycles, the cleaned catalyst was dried at 80 °C in an N_2 environment.

As illustrated in Fig. 11, the Fe_3O_4 NPs demonstrated a stable HGR over six cycles while maintaining a high efficiency. Specifically, the HGR decreased only marginally from 2125.86 ml g_{cat}^{-1} min^{-1} in the first cycle to 2070.0 ml g_{cat}^{-1} min^{-1} in the sixth cycle. This minimal reduction emphasizes the durability and reusability of the catalyst.

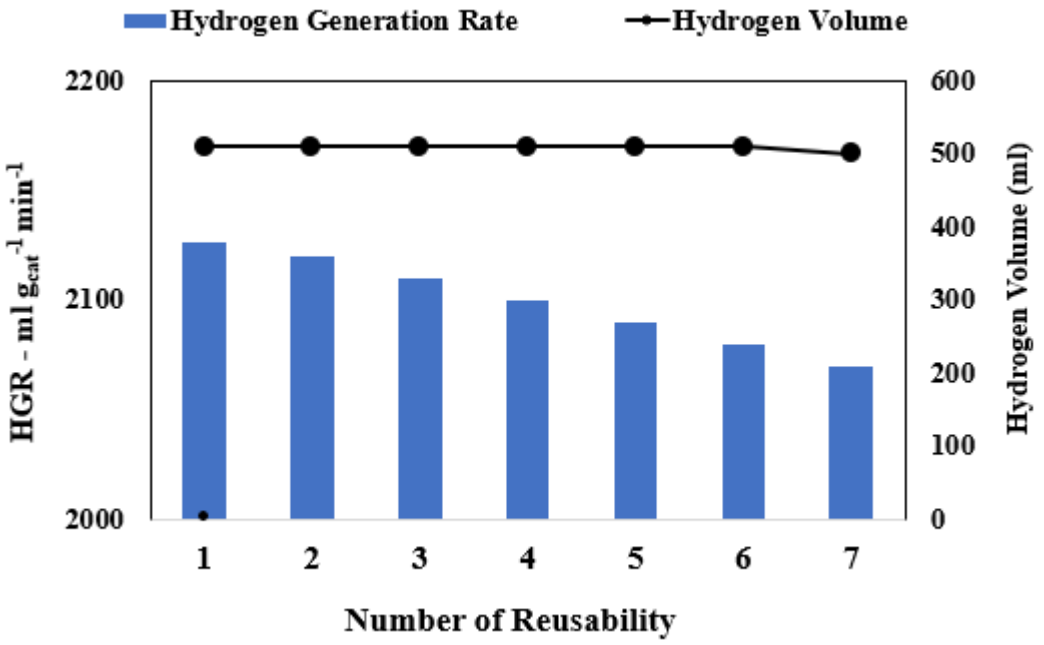

Figure 11. The evolution of hydrogen volume with the number of reusability (1.5% $NaBH_4$, 100 mg catalyst, 30°C)

5. CONCLUSIONS

This study demonstrates the effective use of hydrothermally synthesized Fe_3O_4 nanoparticles (NPs) in $NaBH_4$ methanolysis.

Under optimized conditions of 10% $NaBH_4$ concentration, 100 mg catalyst loading, and a 30°angle, the Fe_3O_4 NPs exhibited an HGR of 2721.9 ml g_{cat}^{-1} min^{-1}. The Ea was determined to be 27.18 kJ mol^{-1}, indicating favorable kinetics at mild temperatures.

XRD analysis revealed a crystallite size of approximately 10.35 nm, with no detectable impurities, highlighting the purity of Fe_3O_4 nanoparticles.

Elemental analysis via EDX confirmed the composition of the nanoparticles, with iron (Fe) and oxygen (O) present in weight percentages of 66.7% and 33.3%, respectively, respectively.

The durability of the catalyst was demonstrated through six consecutive reusability tests, during which 99% of the initial activity was retained after each test. This excellent stability emphasizes its potential for long-term use in industrial hydrogen production processes.

Future research should explore scaling of the synthesis process and evaluate the catalyst performance under industrial conditions to further validate its practical applicability.

Declaration of Ethical Standards

Authors declare to comply with all ethical guidelines, including authorship, citation, data reporting, and original research.

Credit Authorship Contribution Statement

Ayhan Abdullah Ceyhan: Writing – review & editing, Visualization, Validation, Supervision, Resources, Project administration, Methodology, Funding acquisition, Data curation, Conceptualization.

Houssem Lakhali: Writing – original draft, Visualization, Validation, Investigation.

Ömer Şahin: Writing – original draft, Validation, Supervision, Resources, Methodology, Conceptualization.

Declaration of Competing Interest

The authors declare that they have no known competing financial interests or personal relationships that could have appeared to influence the work reported in this paper.

Funding / Acknowledgements

This study was supported by Konya Technical University's Scientific Research Projects (BAP) Coordination Unit (Project No: 221116033).

Data Availability

No datasets were generated or analyzed during the current study

REFERENCES

[1] Ü. Ecer, A. Zengin, and T. Şahan, "Hydrogen generation from $NaBH_4$ hydrolysis catalyzed by cobalt (0)-Deposited cross-linked polymer brushes: Optimization with an experimental design approach," *Int J Hydrogen Energy*, vol. 48, no. 34, pp. 12814–12825, 2023.

[2] Q. Wang, Z. Sun, J. Guo, and R. Li, "The more effective option to combat environmental degradation: Energy efficiency vs. renewable energy vs. natural gas?," *Energy*, vol. 283, p. 128512, 2023.

[3] M. Dragan, "Hydrogen storage in complex metal hydrides $NaBH_4$: Hydrolysis reaction and experimental strategies. Catalysts 2022; 12: 356."

[4] H. Lakhali, A. A. Ceyhan, and Ö. Şahin, "Novel Fe_3O_4@SiO_2/Co-Mo-B core-shell magnetic nanocatalyst: A reusable system for high-performance hydrogen evolution in borohydride hydrolysis," *Inorg Chem Commun*, p. 114406, 2025.

[5] T. E. Dudu and E. Ö. Şeker, "Green Energy Source H_2 Production from $NaBH_4$ Hydrolysis Using p (Oxalic Acid) Based Non-metallic Catalyst," *J Polym Environ*, vol. 31, no. 8, pp. 3445–3453, 2023.

[6] P. Muthukumar *et al.*, "Review on large-scale hydrogen storage systems for better sustainability," *Int J Hydrogen Energy*, 2023.

[7] J. Song, R. Li, and H. Dong, "Controllable hydrogen production from $NaBH_4$ hydrolysis promoted by acetic acid," *Int J Hydrogen Energy*, vol. 48, no. 22, pp. 8093–8100, 2023.

[8] Y. Xia, Y. Pei, Y. Wang, F. Li, and Q. Li, "Effects of various metal doping on the structure and catalytic activity of CoB catalyst in hydrogen production from $NaBH_4$ hydrolysis," *Fuel*, vol. 331, p. 125733, 2023.

[9] S. Demirci, S. D. Sutekin, O. Guven, and N. Sahiner, "Poly (2-aminoethyl methacrylate) based microgels catalyst system to be used in hydrolysis and methanolysis of $NaBH_4$ for H_2 generation," *Int J Hydrogen Energy*, vol. 48, no. 60, pp. 23002–23012, 2023.

[10] E. Fangaj, A. A. Ali, F. Güngör, S. Bektaş, and A. A. Ceyhan, "The use of metallurgical waste sludge as a catalyst in hydrogen production from sodium borohydride," *Int J Hydrogen Energy*, vol. 45, no. 24, pp. 13322–13329, 2020.

[11] K. Ganesan *et al.*, "Catalytic hydrolysis of sodium borohydride for hydrogen production using phosphorylated silica particles," *Environmental Science and Pollution Research*, vol. 30, no. 8, pp. 21199–21212, 2023.

[12] A. Kytsya *et al.*, "Bimetallic Ni-Co nanoparticles as an efficient catalyst of hydrogen generation via hydrolysis of $NaBH_4$," *J Alloys Compd*, vol. 908, p. 164484, 2022.

[13] F. Wang, Y. Wang, Y. Zhang, Y. Luo, and H. Zhu, "Highly dispersed RuCo bimetallic nanoparticles supported on carbon black: enhanced catalytic activity for hydrogen generation from $NaBH_4$ methanolysis," *J Mater Sci*, vol. 53, no. 9, pp. 6831–6841, 2018.

[14] G. M. Arzac and A. Fernández, "Hydrogen production through sodium borohydride ethanolysis,"

Int J Hydrogen Energy, vol. 40, no. 15, pp. 5326–5332, 2015.

[15] H. Ç. Kazıcı, M. S. İzgi, and Ö. Şahin, "Co-Mn-B nanoparticles supported on epoxy-based polymer as catalyst for evolution of H_2 from ammonia borane semi-methanolysis," *J Electron Mater*, vol. 51, no. 5, pp. 2356–2368, 2022.

[16] T. Wang, T. Jiang, H. Zhang, and Y. Zhao, "Advances in catalysts for hydrogen production by methanolysis of sodium borohydride," *Int J Hydrogen Energy*, vol. 47, no. 32, pp. 14589–14610, 2022.

[17] M. Bekirogullari, "Synthesis of waste eggshell-derived Au/Co/Zn/eggshell nanocomposites for efficient hydrogen production from $NaBH_4$ methanolysis," *Int J Hydrogen Energy*, vol. 52, pp. 1380–1389, 2024.

[18] X. Li, N. Yang, X. Cen, S. Li, L. Zhang, and Z.-H. Lu, "Exceptional activity of hollow porphyrin frameworks-confined Ni nanoparticles for hydrogen production from $NaBH_4$ methanolysis," *Fuel*, vol. 354, p. 129332, 2023.

[19] S. Akbar, M. N. Qureshi, and S. A. Khan, "Fabrication of chitosan supported copper nano catalyst for the hydrogen gas production through methanolysis and hydrolysis of $NaBH_4$," *Int J Hydrogen Energy*, vol. 101, pp. 313–322, 2025.

[20] D. Yildiz, "Hydrogen generation from $NaBH_4$ methanolysis with Ru/AC catalyst synthesized by microwave reduction method," *Waste Biomass Valorization*, pp. 1–10, 2024.

[21] S. Prabu and K.-Y. Chiang, "Synergistic effect of Pd-Co_3O_4 nanoparticles supported on coffee-derived sulfur, nitrogen-codoped hierarchical porous carbon for efficient methanolysis of $NaBH_4$," *J Alloys Compd*, vol. 938, p. 168548, 2023.

[22] F. Wang, Y. Zhang, Y. Luo, Y. Wang, and H. Zhu, "Preparation of dandelion-like Co–Mo–P/CNTs-Ni foam catalyst and its performance in hydrogen production by alcoholysis of sodium borohydride," *Int J Hydrogen Energy*, vol. 45, no. 55, pp. 30443–30454, 2020.

[23] P. Dai, Y. Yao, E. Hu, D. Xu, Z. Li, and C. Wang, "Self-assembled ZIF-67@graphene oxide as a cobalt-based catalyst precursor with enhanced catalytic activity toward methanolysis of sodium borohydride," *Appl Surf Sci*, vol. 546, p. 149128, 2021.

[24] Y. Niu *et al.*, "Magnetic Microcapsules Based on Fe_3O_4 Nanoparticles: Preparation, Properties, and Applications," *Mater Today Commun*, p. 108660, 2024.

[25] L. Dong *et al.*, "A review on recent advances in the applications of composite Fe_3O_4 magnetic nanoparticles in the food industry," *Crit Rev Food Sci Nutr*, vol. 64, no. 4, pp. 1110–1138, 2024.

[26] H. Li, S. Yang, D. Hui, and R. Hong, "Progress in magnetic Fe_3O_4 nanomaterials in magnetic resonance imaging," *Nanotechnol Rev*, vol. 9, no. 1, pp. 1265–1283, 2020.

[27] X. Tang, Q. Feng, K. Liu, Z. Li, and H. Wang, "Fabrication of magnetic Fe_3O_4/silica nanofiber composites with enhanced Fenton-like catalytic performance for Rhodamine B degradation," *J Mater Sci*, vol. 53, no. 1, pp. 369–384, 2018.

[28] F. Mirshafiee and M. Rezaei, "Bifunctional CoNi/Fe_3O_4@GO catalyst for hydrogen generation through $NaBH_4$ in different solvolytic environments: The effect of sequential metal introduction," *Int J Hydrogen Energy*, vol. 68, pp. 1108–1118, 2024.

[29] M. Alshammari *et al.*, "Hydrogen catalytic performance of hybrid Fe_3O_4/FeS_2/g-C_3N_4 nanocomposite structures," *Diam Relat Mater*, vol. 138, p. 110214, 2023.

[30] Y. Chi *et al.*, "Synthesis of Fe_3O_4@SiO_2–Ag magnetic nanocomposite based on small-sized and highly dispersed silver nanoparticles for catalytic reduction of 4-nitrophenol," *J Colloid Interface Sci*, vol. 383, no. 1, pp. 96–102, 2012.

[31] J. Li, Y. Xu, W. Hou, and X. Yao, "Loading Fe_3O_4 nanoparticles on N, S co-doped graphene suppressing polysulfides conversion toward high-performance Li–S batteries," *J Mater Sci*, vol. 58, no. 10, pp. 4552–4564, 2023.

[32] A. Khodadadi, M. R. Talebtash, and M. Farahmandjou, "Effect of PVA/PEG-coated Fe_3O_4 nanoparticles on the structure, morphology and magnetic properties," *Physical Chemistry Research*, vol. 10, no. 4, pp. 537–547, 2022.

[33] G. Antarnusa, A. Nene, R. Umam, and P. E. Swastika, "Controlling crystal habit and magnetic

properties of Fe_3O_4 nanoparticles through the stirring velocity for bio-detection applications," *Nano-Structures & Nano-Objects*, vol. 38, p. 101123, 2024.

[34] V. Adimule, B. C. Yallur, M. M. Pai, S. R. Batakurki, and S. S. Nandi, "Biogenic synthesis of magnetic palladium nanoparticles decorated over reduced graphene oxide using piper betle petiole extract (Pd-rGO@ Fe_3O_4 NPs) as heterogeneous hybrid nanocatalyst for applications in suzuki-miyaura coupling reactions of biphenyl compounds," *Top Catal*, pp. 1–14, 2022.

[35] P. Liu, S. Liu, and S.-W. Bian, "Core–shell-structured Fe_3O_4/Pd@ ZIF-8 catalyst with magnetic recyclability and size selectivity for the hydrogenation of alkenes," *J Mater Sci*, vol. 52, no. 20, pp. 12121–12130, 2017.

[36] M. S. Izgi, M. Ş. Ece, H. Ç. Kazici, Ö. Şahïn, and E. Onat, "Hydrogen production by using Ru nanoparticle decorated with Fe_3O_4@ SiO_2–NH_2 core-shell microspheres," *Int J Hydrogen Energy*, vol. 45, no. 55, pp. 30415–30430, 2020.

[37] T. Kamakshi, G. S. Sundari, H. Erothu, and R. S. Singh, "Effect of nickel dopant on structural morphological and optical characteristics of Fe_3O_4 nanoparticles," *Rasayan J. Chem*, vol. 12, no. 2, pp. 531–536, 2019.

[38] M. A. Vargas, J. E. Diosa, and E. Mosquera, "Data on study of hematite nanoparticles obtained from Iron (III) oxide by the Pechini method," *Data Brief*, vol. 25, p. 104183, 2019.

[39] S. Chakroborty *et al.*, "A detailed investigation and catalytic application of gold nanoparticles towards synthesis of N & O-heterocycles," *Top Catal*, vol. 67, no. 1, pp. 123–139, 2024.

[40] D. Kılınç and Ö. Şahin, "Effective polymer decoration on nickel-imine complex to enhance catalytic hydrogen evolution," *Konya Journal of Engineering Sciences*, vol. 12, no. 1, pp. 37–52, 2024.

[41] R. Y. Hong *et al.*, "Preparation, characterization and application of Fe_3O_4/ZnO core/shell magnetic nanoparticles," *Mater Res Bull*, vol. 43, no. 8–9, pp. 2457–2468, 2008.

[42] İ. Küçük and H. Biçiçi, "Adsorption of malachite green into potato peel: nonlinear isotherm and kinetic," *Konya Journal of Engineering Sciences*, vol. 12, no. 1, pp. 150–161, 2024.

[43] E. Kalantari, M. A. Khalilzadeh, and D. Zareyee, "Effective reduction of Cr (VI) and organic dyes using Pd NPs/Fe_3O_4@ nanocellulose as a recoverable catalyst in aqueous media," *J Inorg Organomet Polym Mater*, vol. 31, no. 1, pp. 319–330, 2021.

[44] V. C. Deivayanai, S. Karishma, P. Thamarai, A. Saravanan, and P. R. Yaashikaa, "Artificial neural network modeling for adsorption of Congo red and methylene blue dye removal using pineapple waste-mediated magnetic nanoparticles," *Appl Nanosci*, vol. 15, no. 2, p. 9, 2025.

[45] L. Yunchao, W. Tao, L. Lvdan, L. Guangming, and Z. Guangzhao, "Ion Specificity at a Low Salt Concentration in Water–Methanol Mixtures Exemplified by a Growth of Polyelectrolyte Multilayer," 2013.

[46] C. Saka, "Rapid and robust hydrogen generation from sodium borohydride in optimum mixture of methanol and ethylene glycol using phosphorus-doped chitosan polymer matrix dispersed on alumina nanoparticles," *J Mol Liq*, vol. 401, p. 124654, 2024.

[47] Ö. Şahin, H. Lakhali, and A. A. Ceyhan, "Highly efficient and reusable $CeVO_4$@Fe_3O_4/(Cr–Fe/Co) magnetic nanocatalyst for sustainable hydrogen generation from $NaBH_4$ hydrolysis," *Int J Hydrogen Energy*, vol. 151, p. 150114, 2025.

[48] M. Altınsoy and A. A. Ceyhan, "Synthesis of cobalt-doped catalyst for $NaBH_4$ hydrolysis using eggshell biowaste," *Int J Hydrogen Energy*, vol. 48, no. 72, pp. 28018–28033, 2023.

[49] H. Lakhali, Ö. Şahin, and A. A. Ceyhan, "A novel core–shell Fe_3O_4@ SiO_2/Co–Cr–B magnetic catalyst for efficient and reusable hydrogen evolution from $NaBH_4$ hydrolysis," *New Journal of Chemistry*, 2025.

[50] H. Lakhali, S. Kocaman, G. Ahmetli, and A. A. Ceyhan, "Enhanced hydrogen generation in borohydride hydrolysis using an efficient and reusable IA-CNT supported Co-Mo-B catalyst," *Diam Relat Mater*, p. 112364, 2025.

[51] Ö. Şahin, A. A. Ceyhan, and H. Lakhali, "Core–shell doping of cerium oxide with (Cr–Fe/Co)-B catalyst for enhanced hydrogen evolution in borohydride hydrolysis systems: performance and

catalytic efficiency," *Research on Chemical Intermediates*, vol. 51, no. 5, pp. 2435–2468, 2025.

[52] C. Saka and A. Balbay, "Metal-free catalyst fabrication by incorporating oxygen groups on the surface of the carbonaceous sample and efficient hydrogen production from $NaBH_4$ methanolysis," *Int J Hydrogen Energy*, vol. 47, no. 11, pp. 7242–7251, 2022.

[53] P. Dai, Y. Yao, E. Hu, D. Xu, Z. Li, and C. Wang, "Self-assembled ZIF-67@ graphene oxide as a cobalt-based catalyst precursor with enhanced catalytic activity toward methanolysis of sodium borohydride," *Appl Surf Sci*, vol. 546, p. 149128, 2021.

[54] K. Ramya, K. S. Dhathathreyan, J. Sreenivas, S. Kumar, and S. Narasimhan, "Hydrogen production by alcoholysis of sodium borohydride," *Int J Energy Res*, vol. 37, no. 14, pp. 1889–1895, 2013.

[55] Ş. Karakaya, E. Pehlivan, and A. A. Ceyhan, "Preparation of an efficient and reusable cobalt doped vermiculite ore catalyst for hydrogen production from sodium borohydride," *Int J Hydrogen Energy*, vol. 73, pp. 282–293, 2024.

[56] E. Fangaj and A. A. Ceyhan, "Apricot Kernel shell waste treated with phosphoric acid used as a green, metal-free catalyst for hydrogen generation from hydrolysis of sodium borohydride," *Int J Hydrogen Energy*, vol. 45, no. 35, pp. 17104–17117, 2020.

[57] A. A. Ceyhan, S. Edebali, and E. Fangaj, "A study on hydrogen generation from $NaBH_4$ solution using Co-loaded resin catalysts," *Int J Hydrogen Energy*, vol. 45, no. 60, pp. 34761–34772, 2020.

[58] M. A. Gosalvez and J. Alberdi-Rodriguez, "A microscopic perspective on heterogeneous catalysis," *arXiv preprint arXiv:1812.11398*, 2018.

[59] H. Lakhali, S. Baştaş, A. B. Türkben, and A. A. Ceyhan, "Eco-friendly green synthesis of Co_3O_4-NiO nano catalysts from Papaver somniferum biomass for efficient $NaBH_4$ Hydrolysis: Advancing circular bioeconomy and clean hydrogen energy conversion," *Biomass Bioenergy*, vol. 202, p. 108240, 2025, doi:

[60] S. Anantharaj, P. E. Karthik, and S. Noda, "The significance of properly reporting turnover frequency in electrocatalysis research," *Angewandte Chemie International Edition*, vol. 60, no. 43, pp. 23051–23067, 2021.

[61] F. Mirshafiee and M. Rezaei, "Bifunctional CoNi/Fe_3O_4@GO catalyst for hydrogen generation through $NaBH_4$ in different solvolytic environments: The effect of sequential metal introduction," *Int J Hydrogen Energy*, vol. 68, pp. 1108–1118, 2024.

[62] Ö. Şahin, M. S. İzgi, S. Tayboğa, and H. Ç. Kazıcı, "Effect of plasma pretreatment of Co–Cu–B catalyst on hydrogen generation from sodium borohydride methanolysis," *Reaction Kinetics, Mechanisms and Catalysis*, vol. 133, no. 2, pp. 851–861, 2021.

[63] R. C. Chikate, D. R. Petkar, B. S. Kadu, and A. P. Jakhade, "Fe–Ni/MMT nanocomposites as efficient H_2 generation catalyst: Tandem approach towards one-pot synthesis of secondary amines," *Int J Hydrogen Energy*, vol. 45, no. 56, pp. 31798–31811, 2020.

[64] Y. Zhang, J. Zou, Y. Luo, and F. Wang, "Study on preparation and performance of Ru-Fe/GO catalyst for sodium borohydride alcoholysis to produce hydrogen," *Fullerenes, Nanotubes and Carbon Nanostructures*, vol. 28, no. 10, pp. 786–793, 2020.

[65] J. D. Ocon, T. N. Tuan, Y. Yi, R. L. de Leon, J. K. Lee, and J. Lee, "Ultrafast and stable hydrogen generation from sodium borohydride in methanol and water over Fe–B nanoparticles," *J Power Sources*, vol. 243, pp. 444–450, 2013.